

Thermally induced band hybridization in bilayer-bilayer MoS_2/WS_2 heterostructure

Yanchong Zhao(赵岩翀), Tao Bo(薄涛), Luojun Du(杜罗军), Jinpeng Tian(田金朋), Xiaomei Li(李晓梅), Kenji Watanabe, Takashi Taniguchi, Rong Yang(杨蓉), Dongxia Shi(时东霞), Sheng Meng(孟胜), Wei Yang(杨威), Guangyu Zhang(张广宇)

Citation: Chin. Phys. B, 2021, 30 (**5**): 057801. DOI: 10.1088/1674-1056/abeee3
Journal homepage: http://cpb.iphy.ac.cn; http://iopscience.iop.org/cpb

What follows is a list of articles you may be interested in

Modulation of the second-harmonic generation in MoS_2 by graphene covering

Chunchun Wu(吴春春), Nianze Shang(尚念泽), Zixun Zhao(赵子荀), Zhihong Zhang(张智宏), Jing Liang(梁晶), Chang Liu(刘畅), Yonggang Zuo(左勇刚), Mingchao Ding(丁铭超), Jinhuan Wang(王金焕), Hao Hong(洪浩), Jie Xiong(熊杰), and Kaihui Liu(刘开辉)

Chin. Phys. B, 2021, 30 (**2**): 027803. DOI: 10.1088/1674-1056/abd77f

Visible-to-near-infrared photodetector based on graphene-$MoTe_2$-graphene heterostructure

Rui-Xue Hu(户瑞雪), Xin-Li Ma(马新莉), Chun-Ha An(安春华), Jing Liu(刘晶)

Chin. Phys. B, 2019, 28 (**11**): 117802. DOI: 10.1088/1674-1056/ab4576

Efficient doping modulation of monolayer WS_2 for optoelectronic applications

Xinli Ma(马新莉), Rongjie Zhang(张荣杰), Chunhua An(安春华), Sen Wu(吴森), Xiaodong Hu(胡晓东), Jing Liu(刘晶)

Chin. Phys. B, 2019, 28 (**3**): 037803. DOI: 10.1088/1674-1056/28/3/037803

Raman spectroscopy characterization of two-dimensional materials

Fang Liang(梁芳), Hejun Xu(徐何军), Xing Wu(吴幸), Chaolun Wang(王超伦), Chen Luo(骆晨), Jian Zhang(张健)

Chin. Phys. B, 2018, 27 (**3**): 037802. DOI: 10.1088/1674-1056/27/3/037802

Different angle-resolved polarization configurations of Raman spectroscopy: A case on the basal and edge plane of two-dimensional materials

Xue-Lu Liu(刘雪璐), Xin Zhang(张昕), Miao-Ling Lin(林妙玲), Ping-Heng Tan(谭平恒)

Chin. Phys. B, 2017, 26 (**6**): 067802. DOI: 10.1088/1674-1056/26/6/067802

RAPID COMMUNICATION

Thermally induced band hybridization in bilayer-bilayer MoS_2/WS_2 heterostructure*

Yanchong Zhao(赵岩翀)[1,2,†], Tao Bo(薄涛)[1,3,†], Luojun Du(杜罗军)[4], Jinpeng Tian(田金朋)[1,2], Xiaomei Li(李晓梅)[1,2], Kenji Watanabe[5], Takashi Taniguchi[6], Rong Yang(杨蓉)[1,3,7], Dongxia Shi(时东霞)[1,2,7,‡], Sheng Meng(孟胜)[1,2,3], Wei Yang(杨威)[1,2,3,7,§], and Guangyu Zhang(张广宇)[1,2,3,7,¶]

[1] *Beijing National Laboratory for Condensed Matter Physics; Key Laboratory for Nanoscale Physics and Devices, Institute of Physics, Chinese Academy of Sciences, Beijing* 100190, *China*

[2] *School of Physical Sciences, University of Chinese Academy of Sciences, Beijing* 100190, *China*

[3] *Songshan Lake Materials Laboratory, Dongguan* 523808, *China*

[4] *Department of Electronics and Nanoengineering, Aalto University, Tietotie* 3, *FI*-02150, *Finland*

[5] *Research Center for Functional Materials, National Institute for Materials Science*, 1-1 *Namiki, Tsukuba* 305-0044, *Japan*

[6] *International Center for Materials Nanoarchitectonics, National Institute for Materials Science, 1-1 Namiki, Tsukuba* 305-0044, *Japan*

[7] *Beijing Key Laboratory for Nanomaterials and Nanodevices, Beijing* 100190, *China*

(Received 3 March 2021; revised manuscript received 12 March 2021; accepted manuscript online 16 March 2021)

Transition metal dichalcogenides (TMDs), being valley selectively, are an ideal system hosting excitons. Stacking TMDs together to form heterostructure offers an exciting platform to engineer new optical and electronic properties in solid-state systems. However, due to the limited accuracy and repetitiveness of sample preparation, the effects of interlayer coupling on the electronic and excitonic properties have not been systematically investigated. In this report, we study the photoluminescence spectra of bilayer-bilayer MoS_2/WS_2 heterostructure with a type II band alignment. We demonstrate that thermal annealing can increase interlayer coupling in the van der Waals heterostructures, and after thermally induced band hybridization such heterostructure behaves more like an artificial new solid, rather than just the combination of two individual TMD components. We also carry out experimental and theoretical studies of the electric controllable direct and indirect infrared interlayer excitons in such system. Our study reveals the impact of interlayer coupling on interlayer excitons and will shed light on the understanding and engineering of layer-controlled spin-valley configuration in twisted van der Waals heterostructures.

Keywords: two-dimensional materials, transition metal dichalcogenides (TMDs) heterostructure, band hybridization, interlayer exciton

PACS: 78.66.–w, 73.40.–c

DOI: 10.1088/1674-1056/abeee3

1. Introduction

Monolayer transition metal dichalcogenides (TMDs) are an atomically thin semiconductor with inversion asymmetry and strong spin–orbit coupling (SOC),[1] the associated spin- and valley-dependent selection rules result in a plethora of unique optical properties.[2–4] By stacking TMDs heterostructures with a type II band alignment,[5–7] it favors ultrafast charge transfer of electrons and holes to different layers after optical excitation, and eventually leads to a formation of long-lived interlayer exciton in the low energy range.[8,9] Recent focus has been placed on finding and understanding the collective behaviors induced by the strong electronic interactions in this system. Similar to twisted bilayer graphene,[10,11] twisted TMDs structures offer an unique platform to engineer the electronic band structure and the emergent optical properties.[9,12–14] Though excitonic effects and optical spectra have been studied in many experiments, the results vary greatly even for the same type TMDs heterostructure. The observed phenomenon disunion in experiments strongly suggests a delicate interplay between the crystal lattice, interlayer coupling, band hybridization, and moiré effect in the heterostructures.[9,14–22] A feasible way to engineer such interplay as well as the electronic/optical properties of TMDs heterostructures is badly in need for the application in the area of optoelectronics and valleytronics.

Here we study the photoluminescence (PL) spectra of near 0° aligned bilayer-bilayer MoS_2/WS_2 heterostructures,

*Project supported by the National Key Research and Development Program of China (Grant No. 2020YFA0309604), the National Natural Science Foundation of China (Grant Nos. 11834017, 61888102, and 12074413), the Strategic Priority Research Program of Chinese Academy of Sciences (Grant Nos. XDB30000000 and XDB33000000), the Key-Area Research and Development Program of Guangdong Province, China (Grant No. 2020B0101340001), and the Research Program of Beijing Academy of Quantum Information Sciences (Grant No. Y18G11).

†These authors contributed equally to this work.

‡Corresponding author. E-mail: dxshi@aphy.iphy.ac.cn

§Corresponding author. E-mail: wei.yang@iphy.ac.cn

¶Corresponding author. E-mail: gyzhang@iphy.ac.cn

© 2021 Chinese Physical Society and IOP Publishing Ltd

and demonstrate thermal annealing as an effective means to induce hybridization effects in commensurate van der Waals heterostructures. By employing thermal annealing, we observe a more efficient interlayer charge transfer in the heterostructure indicating a stronger interlayer coupling. Moreover, the PL spectra in the low energy range undergo the transition from multiplet narrow emissions dominated by periodic moiré potential to a couple of emissions dominated by hybridized electronic states. The electric controllability and valley-dependent polarization of the interlayer exciton are also revealed. Our results indicate that after thermally induced band hybridization the heterostructure behaves more like an artificial new solid, rather than just the combination of two individual TMD components.

2. Sample preparation

Figure 1(a) shows a schematic diagram of our device, we prepare h-BN encapsulated near 0° aligned bilayer-bilayer MoS_2/WS_2 heterostructure with few-layer graphene (FLG) as top gate by van der Waals-mediated dry transfer approach employing propylene carbonate (PC) stamp.[23,24] Firstly, FLG, h-BN, bilayer MoS_2, and bilayer WS_2 flakes are exfoliated onto SiO_2 (300 nm)/Si substrate. And then PC stamps are used to pick up h-BN flake, bilayer MoS_2, bilayer WS_2, and another h-BN flake in sequence with accurate alignment based on an optical microscope. The sandwiched structure is then transferred onto SiO_2 (300 nm)/Si substrate, and finally another FLG is transferred on it as a top gate by dry transfer technique. Finally, metal contacts to the heterostructure and FLG are patterned by the standard micro-fabrication processes including e-beam lithography (EBL), metal evaporation Ti (3 nm)/Au (40 nm), and lifting-off. Figure 1(b) shows an optical image of the device, where the bilayer MoS_2 and bilayer WS_2 are sketched by red and black dotted lines, respectively.

3. Results and discussion

Micro-photoluminescence (PL) measurements are performed on the as-prepared heterostructure, the sample is held at 10 K and excited under a continuous-wave 532 nm laser with a spot size of 1.5 μm. The blue curve in Fig. 1(c) shows the PL spectra in the energy range of intralayer excitons. The heterostructure shows three dominated PL peaks, which we attribute to the indirect exciton of bilayer MoS_2 or WS_2 (∼ 1.53 eV), neutral A exciton (A^0) of WS_2 (∼ 1.98 eV), A^0 and its negatively charged exciton (A^0) of bilayer MoS_2 (∼ 1.92 eV), respectively. The blue curve in Fig. 1(d) shows the PL spectra in the energy range of interlayer excitons for the twisted bilayer-bilayer MoS_2/WS_2 heterostructure. By using Gaussian functions to fit the spectra we get multiplet emissions from several nearly equally spaced interlayer exciton resonances, and the averaged full width at half maximum (FWHM) of the emissions is 22.4 meV, these behaviors are the signature of interlayer excitons trapped in moiré potential (Fig. S1). Our results demonstrate that except for monolayer-monolayer case, moiré interlayer exciton can also manifest in the twisted bilayer-bilayer TMDs heterostructure.

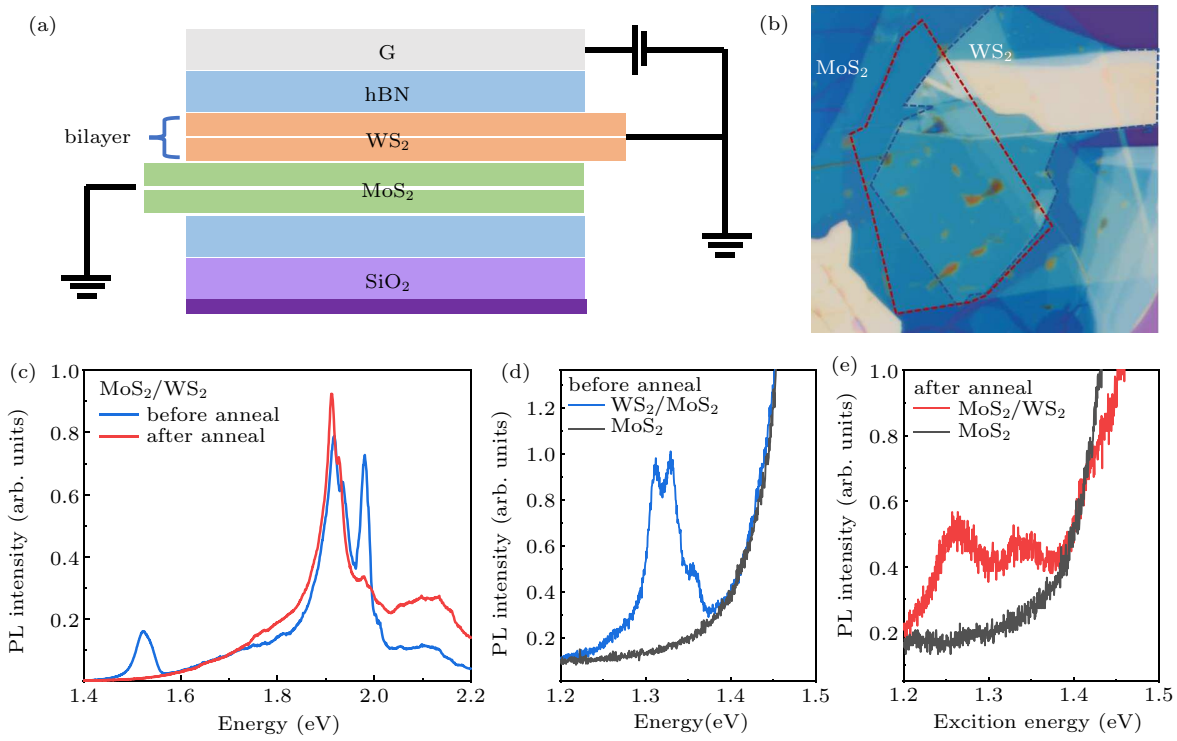


Fig. 1. (a) Schematic diagram for the bilayer-bilayer MoS_2/WS_2. (b) Optical image of the heterostructure. (c) Low temperature PL spectra of intralayer excitons for bilayer-bilayer MoS_2/WS_2 heterostructure before and after thermal annealing. (d), (e) Low temperature PL spectra of interlayer excitons before and after thermal annealing, respectively.

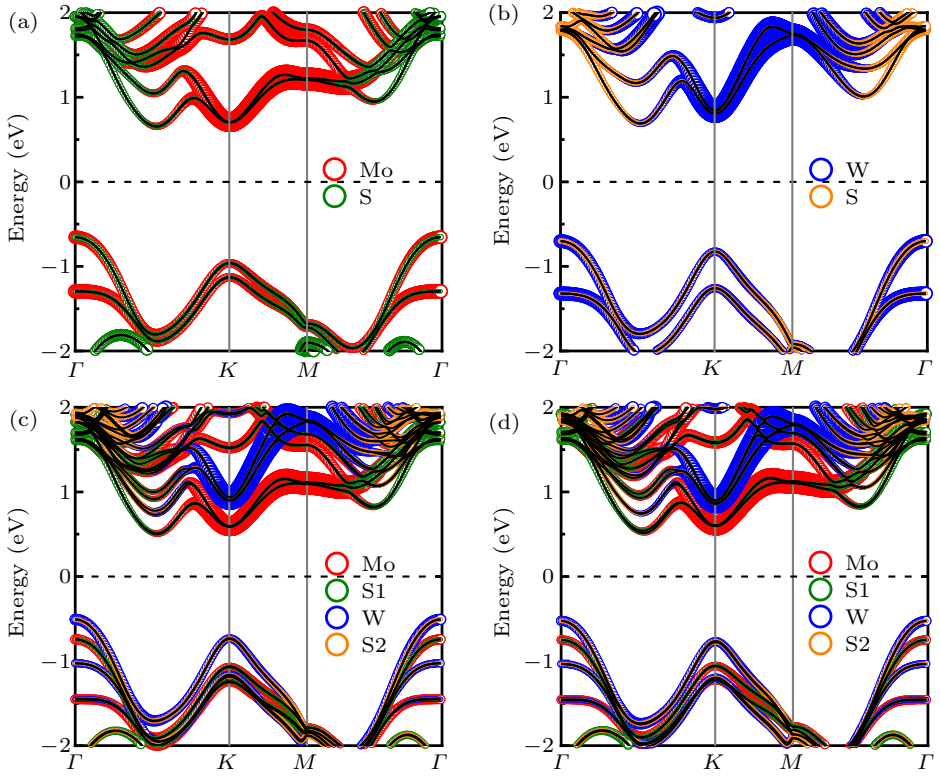


Fig. 2. (a), (b) Calculated band structure of bilayer MoS_2 and WS_2 with orbital analysis in presence of SOC, respectively. (c), (d) Calculated band structure of 0° and 180° twist angle bilayer-bilayer MoS_2/WS_2 heterostructures with orbital analysis in presence of SOC, respectively.

In order to study the influence of thermal annealing on the electronic band structure and light–matter interaction of the heterostructure, we anneal the sample in the Ar/H_2 atmosphere at 300 °C and then perform PL measurements. The red curve in Fig. 1(c) shows the exciton PL spectrum after thermal annealing in the intralayer range. The emission intensities of WS_2 A^0 exciton ($\sim$ 1.98 eV) as well as the intralayer indirect exciton ($\sim$ 1.53 eV) are drastically quenched, indicating a stronger interlayer coupling and more efficient interlayer charge transfer. Moreover, the multiplet emissions of the interlayer excitons (Fig. 1(d)) vanish after thermal annealing, instead two prominent PL peaks emerge with energy red shift as shown in Fig. 1(e). The two emerging peaks show much larger line width and weaker intensity, distinct from the emission of moiré exciton whose line width is relative narrow. Besides, we perform the PL measurement at different sites of the sample, such two peaks can be detected throughout the heterostructure (Fig. S2), suggesting such transition induced by thermal annealing is universal.

PL spectroscopy tools give access to details of the electronic band structure of the heterostructure, the distinct behavior of intra- and inter-layer excitons before and after thermal annealing indicates that thermal annealing alters the interlayer coupling of the van der Waals heterostructure and greatly induces band hybridization. Note that thermally induced rotation has been demonstrated in graphene/h-BN system.[25] Similarly, one can expect that two small angle twisted bilayers studied here will tend to align with each other during thermal annealing. Significantly, due to the small lattice mismatch between MoS_2 and WS_2, the heterostructure will be commensurate at near 0° (180°) twist angle, with the smallest layer separation and nearly ideal R-type (H-type) stacking geometries that free of moiré effect (Fig. S3). Moreover, the increased interlayer coupling will induce giant hybridization, the hybridization strongly modifies the bands structure and induces band shift, as a consequence, the heterostructure behaves more like a new solid rather than just the combination of two individual TMD components.

To better understand the hybridized band structure of the bilayer-bilayer MoS_2/WS_2 heterostructure, we perform density wave functional theory (DFT) calculation. The band structures of pristine bilayer MoS_2 (WS_2) are shown in Figs. 2(a) and 2(b), where an indirect band gap of 1.31 eV (1.39 eV) is consistent with literature.[26–28] Similarly, the band structure of a closely aligned bilayer-bilayer MoS_2/WS_2 heterostructure is calculated and shown in Figs. 2(c) and 2(d) for 0° and 180°, respectively. The calculated results show typical type II band alignment with charges distributed in different layers, and no obvious difference is found between the two alignments. Crucially, the interlayer coupling results giant interlayer hybridization so the band structure of the heterostructure is not merely the superposition of the two components. Unlike monolayer MoS_2/WS_2 heterostructure that has been studied widely, the optical transition of interlayer exciton in bilayer-bilayer MoS_2/WS_2 heterostructure is more complicated due to the presence of multiple indirect transitions at high symmetry

points in the Brillouin zone. The electrons prefer to stay at K_c and Q_c valley of the conduction band (Q_c is the energy minimum along K_c to Γ_c), while the holes tend to occupy the Γ_v and K_v valley of the valance band, giving rise to multiple relaxation paths of interlayer exciton. Specifically, there are three possible indirect transitions, i.e., Γ_v–Q_c, Γ_v–K_c, K_v–Q_c, and one direct K_v–K_c transition. Hence, the observed two prominent interlayer excitons in bilayer-bilayer MoS_2/WS_2 heterostructure after thermal annealing might correspond to different intrinsic relaxion transitions with electrons and holes residing in different valleys of the Brillouin zone.

The spatially indirect interlayer exciton possesses an out-of- plane electric dipole and can couple to the static electric field. When applying a vertical electric field E, an interlayer exciton exhibits linear Stark shifts, and the magnitude of the Stark shift is given by $\Delta = \mu E$, where $\mu = ed$ is the intrinsic dipole moment and d is the vertical displacement of the electron–hole pairs.[29] As the wavefunction distributions of electrons and holes are quite different at each critical point in the Brillouin zone, the electron–hole separations for interlayer excitons with different transitions have corresponding variational parameters. Therefore, it is an effective way to distinguish the transition paths of interlayer excitons by comparing their dipole-moment values.

Figure 3(a) shows the PL spectra at different top gate voltages, and their interlayer nature is revealed from the Stark effect in the linear shift of the peak (black dotted line in Fig. 3(b)). Labeled as IX1 and IX2, the two interlayer excitons exhibit significantly different linear slops of Stark shift (Fig. 3(b)). The IX1 is red shifted from 1.34 eV to 1.21 eV while IX2 is from 1.35 eV to 1.29 eV as the top gate voltage is changed from 6 V to −4 V. This clearly indicates that the two interlayer excitons are distinct with different dipole-moments as well as different electron–hole separations. In our experiments the ratio of μ between IX1 and IX2 is 2.1, estimated from the dashed lines in Fig. 3(b). It should be noted that the top gate will not only induce an out of plane electric field but will also modulate the charge density of the heterostructure leading to the variation of the PL intensity.

Comparing the experimental data to the DFT calculation, we ascribe IX1 and IX2 to K_v–K_c and K_v–Q_c transitions, respectively. We firstly rule out the Γ_v–Q_c and Γ_v–K_c indirect transitions, whose gaps are 1.01 eV and 1.1 eV, respectively. This is because given the large binding energy ($\sim$ 0.2 eV) of interlayer exciton in TMD heterostructures,[30,31] the exciton energy of Γ_v–Q_c and Γ_v–K_c transition is so small ($<$ 1 eV) that beyond our detection range. According to the previous results in twisted monolayer-monolayer MoS_2/WS_2 heterostructure, the ratio of the Stark shift for K_v–K_c to that for K_v–Q_c is around 2.39, which agrees well with the ratio of IX1 to IX2. In this regard, we tentatively assign the interlayer IX1 and IX2 to K_v–K_c and K_v–Q_c transitions, respectively.

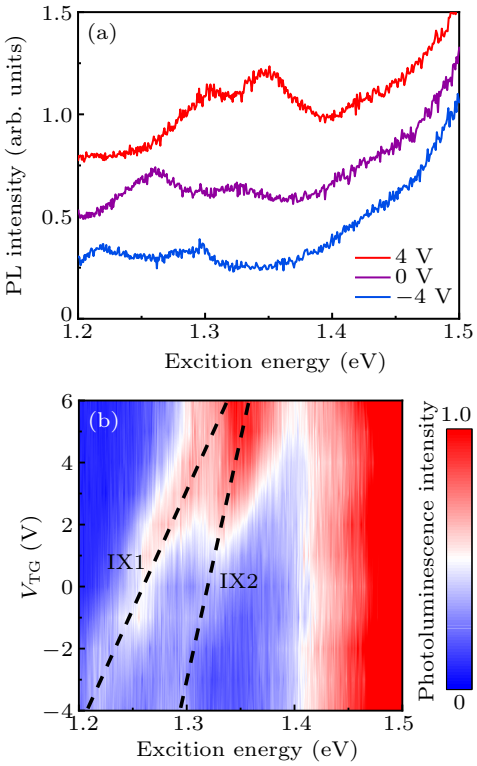


Fig. 3. (a) Gate dependence of the interlayer excitons under 532 nm excitation. (b) Color map of interlayer excitons photoluminescence as a function of applied gate voltage. The black dashed lines are guides to the eye indicating the Stark shift of interlayer excitons IX1 and IX2.

To further confirm the origin of IX1 and IX2, we perform polarization-resolved PL spectra and study their valley-dependent polarization selection rules. Figures 4(a) and 4(c) (4(b) and 4(d)) show the polarization-resolved PL spectra of interlayer (intralayer) excitons at 10 K, excited by 532 nm circularly polarized light. It is clearly shown that the interlayer excitons possess robust negative circular polarization, whereas the intralayer A^0 and A^- excitons have the positive dichroism, indicating the opposite chirality between them. More significantly, IX1 is totally suppressed and indistinguishable with background under co-circularly polarized detection. We thus quantify them by the degree of circular polarization, defined as $P_c = (I_+ - I_-)/(I_+ + I_-)$, where I_+ (I_-) denotes the intensity of the co-polarized (cross-polarized) PL component with the excitation. While IX2 shows relatively small negative circular polarization, IX1 gives giant negative circular polarization that exceeds 65% (inset of Figs. 4(a) and 4(c)).

Such distinct difference of circular polarization between IX1 and IX2 can be interpreted as a result of their relaxation paths, which also confirms our expectation on their origin. Circular polarization is locked with the spin polarization in the heterostructures, and it varies dramatically between different stacking order at atomic scale and different valley of the Brillouin zone.[32] For both the conduction and valance bands around K valley, the corresponding Bloch wavefunctions are

in-plane, predominantly from the d orbitals of Mo and W atoms. Consequently, interlayer hopping between the upper and lower layers is small, which, together with site dipole-field, largely enhances the spin-polarization effects. Therefore, the IX1 exciton, which corresponds to the transition between K_v and K_c valleys, exhibits large circular polarization. However, the IX2 corresponds to the transition between K_v and Q_c valleys, as the considerable out of plane p_z character of chalcogens at Q valleys leads to significant interlayer hopping and seriously weakens the spin-polarization, which gives rise to the exhibiting relatively small circular polarization.[33–35]

At last, we point out that, compared with monolayer-monolayer case,[36] in bilayer-bilayer TMD heterostructure layer number as a new degree of freedom will bring more unique phenomenon to the system. Apart from the layer dependent band structure, which will bring infrared direct- and indirect-interlayer excitons that we have demonstrated here, electric modulated spatial wavefunction distributions of the bounded electrons and holes between the layers are also expected. Such controllability under the quantum confined regime combining with the spin-layer locking effect makes bilayer-bilayer TMDC heterostructure a promising platform to study Bose–Einstein condensation and dissipationless exciton.

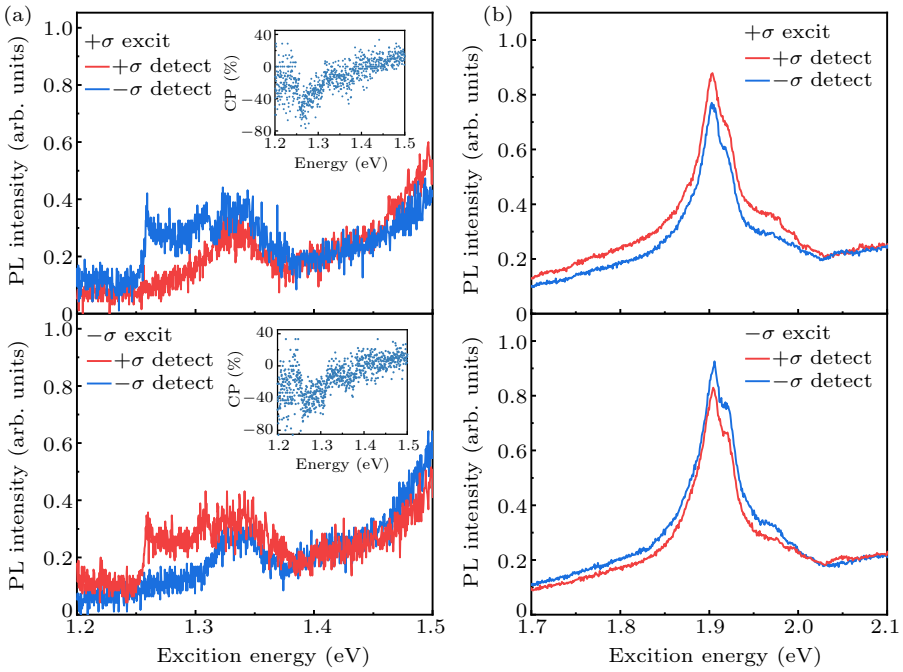


Fig. 4. Polarization-resolved PL spectra near the interlayer (a) and intralayer (b) excitons of the bilayer-bilayer MoS_2/WS_2 heterostructure using $+\sigma$ (top) and $-\sigma$ (bottom) excitation of 532 nm. The insets in (a) show the calculated circular polarization of interlayer excitons.

4. Conclusion and perspectives

In conclusion, we demonstrate that thermal annealing can increase interlayer coupling in the van der Waals heterostructures, and after thermally induced band hybridization such heterostructure behaves more like an artificial new solid, rather than just the combination of two individual TMD components. We carry out experimental and theoretical studies of excitons in near 0° aligned bilayer-bilayer MoS_2/WS_2 heterostructure with strong interlayer coupling, demonstrate the electric controllable direct and indirect infrared interlayer excitons in such system. Our results reveal the impact of interlayer coupling on the excitonic properties of van der Waals heterostructures, and will also shed light on the understanding and engineering of spin-valley configuration in such system.

References

[1] Xiao D, Liu G B, Feng W, Xu X and Yao W 2012 *Phys. Rev. Lett.* **108** 196802
[2] Mak K F, He K, Shan J and Heinz T F 2012 *Nat. Nanotechnol.* **7** 494
[3] Zeng H, Dai J, Yao W, Xiao D and Cui X 2012 *Nat. Nanotechnol.* **7** 490
[4] Zhu B, Zeng H, Dai J, Gong Z and Cui X 2014 *Proc. Natl. Acad. Sci. USA* **111** 11606
[5] Kang J, Tongay S, Zhou J, Li J and Wu J 2013 *Appl. Phys. Lett.* **102** 012111
[6] Terrones H, López-Urías F and Terrones M 2013 *Sci. Rep.* **3** 1
[7] Kośmider K and Fernández-Rossier J 2013 *Phys. Rev. B* **87** 075451
[8] Hong X, Kim J, Shi S F, Zhang Y, Jin C, Sun Y, Tongay S, Wu J, Zhang Y and Wang F 2014 *Nat. Nanotechnol.* **9** 682
[9] Rivera P, Schaibley J R, Jones A M, Ross J S, Wu S, Aivazian G, Klement P, Seyler K, Clark G and Ghimire N J 2015 *Nat. Commun.* **6** 1
[10] Cao Y, Fatemi V, Demir A, Fang S, Tomarken S L, Luo J Y, Sanchez-Yamagishi J D, Watanabe K, Taniguchi T and Kaxiras E 2018 *Nature* **556** 80
[11] Cao Y, Fatemi V, Fang S, Watanabe K, Taniguchi T, Kaxiras E and Jarillo-Herrero P 2018 *Nature* **556** 43
[12] Yu H, Wang Y, Tong Q, Xu X and Yao W 2015 *Phys. Rev. Lett.* **115** 187002
[13] Yu H, Liu G, Tang J, Xu X and Yao W 2017 *Sci. Adv.* **3** e1701696
[14] Okada M, Kutana A, Kureishi Y, Kobayashi Y, Saito Y, Saito T, Watanabe K, Taniguchi T, Gupta S and Miyata Y 2018 *ACS Nano* **12** 2498
[15] Jin C, Regan E C, Yan A, Utama M I B, Wang D, Zhao S, Qin Y, Yang S, Zheng Z and Shi S 2019 *Nature* **567** 76

[16] Tran K, Moody G, Wu F, Lu X, Choi J, Kim K, Rai A, Sanchez D A, Quan J and Singh A 2019 *Nature* **567** 71
[17] Seyler K L, Rivera P, Yu H, Wilson N P, Ray E L, Mandrus D G, Yan J, Yao W and Xu X 2019 *Nature* **567** 66
[18] Alexeev E M, Ruiz-Tijerina D A, Danovich M, Hamer M J, Terry D J, Nayak P K, Ahn S, Pak S, Lee J and Sohn J I 2019 *Nature* **567** 81
[19] Rivera P, Yu H, Seyler K L, Wilson N P, Yao W and Xu X 2018 *Nat. Nanotechnol.* **13** 1004
[20] Kiemle J, Sigger F, Lorke M, Miller B, Watanabe K, Taniguchi T, Holleitner A and Wurstbauer U 2020 *Phys. Rev. B* **101** 121404
[21] Karni O, Barré E, Lau S C, Gillen R, Ma E Y, Kim B, Watanabe K, Taniguchi T, Maultzsch J and Barmak K 2019 *Phys. Rev. Lett.* **123** 247402
[22] Kunstmann J, Mooshammer F, Nagler P, Chaves A, Stein F, Paradiso N, Plechinger G, Strunk C, Schüller C and Seifert G 2018 *Nat. Phys.* **14** 801
[23] Pizzocchero F, Gammelgaard L, Jessen B S, Caridad J M, Wang L, Hone J, Boggild P and Booth T J 2016 *Nat. Commun.* **7** 11894
[24] Zomer P J, Guimarães M H D, Brant J C, Tombros N and van Wees B J 2014 *Appl. Phys. Lett.* **105** 013101
[25] Wang D, Chen G, Li C, Cheng M, Yang W, Wu S, Xie G, Zhang J, Zhao J and Lu X 2016 *Phys. Rev. Lett.* **116** 126101
[26] Cheiwchanchamnangij T and Lambrecht W R L 2012 *Phys. Rev. B* **85** 205302
[27] Zhao W, Ghorannevis Z, Chu L, Toh M, Kloc C, Tan P H and Eda G 2013 *ACS Nano* **7** 791
[28] Zhao W, Ribeiro R M, Toh M, Carvalho A, Kloc C, Castro Neto A H and Eda G 2013 *Nano Lett.* **13** 5627
[29] Miller D A B, Chemla D S, Damen T C, Gossard A C, Wiegmann W, Wood T H and Burrus C A 1984 *Phys. Rev. Lett.* **53** 2173
[30] Wilson N R, Nguyen P V, Seyler K, Rivera P, Marsden A J, Laker Z P, Constantinescu G C, Kandyba V, Barinov A, Hine N D, Xu X and Cobden D H 2017 *Sci. Adv.* **3** e1601832
[31] Van der Donck M and Peeters F M 2018 *Phys. Rev. B* **98** 115104
[32] Yu H, Liu G B and Yao W 2018 *2D Mater.* **5** 035021
[33] Zhu B, Zeng H, Dai J, Gong Z and Cui X 2014 *Proc. Natl. Acad. Sci. USA* **111** 11606
[34] Jones A M, Yu H, Ross J S, Klement P, Ghimire N J, Yan J, Mandrus D G, Yao W and Xu X 2014 *Nat. Phys.* **10** 130
[35] Wang G, Marie X, Bouet L, Vidal M, Balocchi A, Amand T, Lagarde D and Urbaszek B 2014 *Appl. Phys. Lett.* **105** 182105
[36] Cheng Y, Huang C, Hong H, Zhao Z and Liu K 2019 *Chin. Phys. B* **28** 107304